Rapid Growth of α-Ga_2O_3 by HCl-Boosted Halide Vapor Phase Epitaxy and Effect of Precursor Supply Conditions on Crystal Properties

Yuichi Oshima,[1,a)] Katsuaki Kawara,[2] Takayoshi Oshima,[2] Mitsuru Okigawa,[2] Takashi Shinohe[2]

[1]Optical Single Crystals Group, National Institute for Materials Science, 1-1 Namiki, 305-0044 Tsukuba, Japan

[2]FLOSFIA, Inc., Kyodai-Katsura Venture Plaza, 615-8245 Kyoto, Japan

a) Corresponding author: OSHIMA.Yuichi@nims.go.jp

Abstract

We investigated the effect of supply conditions of GaCl, O_2, and additional HCl on the growth rate of (0001) α-Ga_2O_3 by halide vapor phase epitaxy and the crystal properties. The parasitic gas-phase reaction was markedly suppressed by supplying HCl gas in addition to GaCl and O_2, and a rapid growth rate as high as 101 μm/h was achieved. Thermodynamic analysis revealed that the addition of HCl works to convert GaCl into $GaCl_3$, and it was elucidated that the parasitic gas-phase reaction was suppressed because α-Ga_2O_3 was grown through the chemical reaction of $GaCl_3$ and the oxygen sources (O_2 and/or H_2O), the equilibrium constant of which is much smaller than that when GaCl is used. The full-width at half-maximum of the X-ray rocking curve of $10\bar{1}2$ diffraction measured in skew-symmetric geometry decreased with increasing growth rate by increasing the precursor supply, whereas that of symmetric *0006* diffraction did not show a systematic tendency. H and Cl impurities

were detected in the unintentionally doped epilayers by secondary ion mass spectrometry. [Cl] increased rapidly with increasing growth rate, reaching 1.4×10^{18} cm^{-3} at 101 μm/h. The VI/III ratio difference did not have a significant effect on [H] or [Cl]. α-Ga_2O_3 islands were formed through selective area growth, and the lateral/vertical growth rate ratio decreased with increasing growth rate.

Keywords: halide vapor phase epitaxy, gallium oxide, metastable

1. Introduction

Corundum-structured α-Ga_2O_3 is an ultra-wide bandgap semiconductor with a bandgap energy of E_g = 5.3 eV [1]. α-Ga_2O_3 is promising for power device applications because of its very large bandgap, and Schottky barrier diodes (SBDs) with very low on-resistance have been prepared. The on-resistance/breakdown voltage of the SBDs were 0.1 mΩcm^2/531 V and 0.4 mΩcm^2/855 V [2]. α-Ga_2O_3 forms solid solutions with other corundum oxide families because of its ordinary crystal structure. For example, α-$(Al_xGa_{1-x})_2O_3$ can be grown without compositional limitation [3] unlike β-$(Al_xGa_{1-x})_2O_3$ [4]. Such solid solutions and their heterostructures are promising for the development of high-performance devices. It is difficult to prepare α-Ga_2O_3 with *p*-type conductivity, similar to the case of β-Ga_2O_3. However, corundum-structured *p*-type oxides such as α-Ir_2O_3 are available to form a hetero *pn*-junction [5], and metal-oxide-semiconductor field-effect transistors (MOSFETs) with a *p*-type well layer have been prepared [6].

To realize high-performance and practical α-Ga_2O_3 power devices, we need to develop an epitaxial

growth technique that enables the growth of high-quality α-Ga_2O_3 films with controlled electrical conductivity at a reasonably low production cost. Mist chemical vapor deposition (mist-CVD) [1, 5] and halide vapor phase epitaxy (HVPE) [7-9] have been shown to be promising approaches. Molecular beam epitaxy (MBE) [10, 11] and metalorganic chemical vapor deposition (MOCVD) [12] have also been investigated; however, a breakthrough in these methods is required to grow phase-pure thick α-Ga_2O_3 films. Currently, virtually all the reported α-Ga_2O_3 devices are based on mist-CVD grown films. HVPE, the target growth technique of the present work, is characterized by a rapid growth rate and high purity of the resulting crystals. HVPE of α-Ga_2O_3 is therefore promising for the growth of thick drift layers or the fabrication of freestanding α-Ga_2O_3 wafers. Indeed, we have demonstrated very large growth rates of α-Ga_2O_3 of over 100 μm/h [7]. Furthermore, we observed that supplying HCl gas in addition to GaCl and O_2 precursors dramatically increased the growth rate. However, the effect of the additional HCl has not been investigated systematically, and the mechanism is not well understood. Furthermore, the effects of precursor supply conditions and the growth rate on the properties of the grown films have not yet been clarified in the presence of additional HCl.

Improvement of the crystal quality is also one of the most important technical issues for α-Ga_2O_3. α-Ga_2O_3 is the high-pressure stable phase of Ga_2O_3 and is metastable under ambient pressure [13], similar to diamond. Therefore, melt-grown native substrates are not available, similar to the case for most wide-bandgap semiconductors. Accordingly, α-Ga_2O_3 films are heteroepitaxially grown, usually

on sapphire substrates. The dislocation density of such α-Ga_2O_3 films is typically as high as 10^{10} cm^{-2} because of the large lattice mismatch [14]. Although we have demonstrated the remarkable reduction of dislocation density to less than 5×10^6 cm^{-3} by epitaxial lateral overgrowth (ELO) [14], the technique remains in its infancy. To further improve the ELO technique, it is essential to clarify the growth behavior of the α-Ga_2O_3 islands.

In the present work, we systematically investigated the effect of additional HCl supply on the HVPE growth rate of α-Ga_2O_3, and thermodynamic analysis was utilized to clarify the mechanism. We have also investigated how precursor supply conditions under the existence of additional HCl affects the growth characteristics and crystal properties, including ELO-grown α-Ga_2O_3 island morphology. To further improve the crystal quality of α-Ga_2O_3 by HVPE and to apply the technique to device mass production, it is essential to understand the basic growth characteristics and background mechanisms. We believe that this report greatly contributes to that objective.

2. Experimental

HVPE of α-Ga_2O_3 was performed in a lab-made horizontal quartz reactor (Fig. 1) at atmospheric pressure. $GaCl_x$ and O_2 (>99.99995% pure) were supplied as the gallium and oxygen precursors, respectively. N_2 was used as the carrier gas (dew point < −110°C). The temperatures of the growth zone and Ga source zone were fixed at 520°C and 570°C, respectively. $GaCl_x$ was synthesized by the chemical reaction of Ga metal (>99.99999% pure) and HCl gas (>99.999% pure) in the Ga source

zone. The conversion efficiency was very high, and virtually 100% of the HCl gas was consumed to produce $GaCl_x$. GaCl is dominantly produced through the reaction when the temperature is sufficiently high, whereas $GaCl_3$ is dominant at low temperatures. Thermodynamic analysis indicated that more than 98% of the $GaCl_x$ should be GaCl at 570°C [7]. Indeed, no significant changes in the growth rate of α-Ga_2O_3 were observed when the Ga source zone temperature was increased, indicating that the molar fraction of GaCl was almost saturated at 570°C. Accordingly, we assumed that the flow rate of GaCl from the Ga container (denoted as F_0(GaCl)) was equal to that of the HCl gas supply into the Ga container. The HVPE apparatus was equipped with an additional gas line outside the Ga container, which supplied HCl gas (the flow rate is denoted by F_0(HCl)) without contacting Ga metal. This additional HCl gas plays a critical role in realizing high-speed growth, as mentioned in the introduction. The GaCl and additional HCl were transferred to the growth zone separately from the O_2 gas (the flow rate is denoted by $F_0(O_2)$). The sum of F_0(GaCl), F_0(HCl), and the carrier gas flow rate was fixed at 3 slm. The sum of $F_0(O_2)$ and the carrier gas flow rate was fixed at 5 slm.

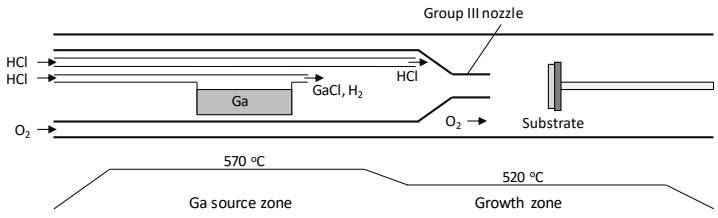

Figure 1. Schematic illustration of HVPE reactor and temperature profile.

An α-Ga_2O_3 epilayer was grown on a *c*-plane sapphire substrate under the growth conditions described above to investigate the effect of the gas flow conditions. Each growth was performed in two steps. First, an approximately 0.3-μm-thick α-Ga_2O_3 layer was grown at 12 μm/h (F_0(GaCl) = 10 sccm, F_0(HCl) = 10 sccm, $F_0(O_2)$ = 100 sccm); then, the gas flow rates were switched to those of the target condition for the second layer. The thickness of the second layer was fixed at approximately 3 μm. The growth rate was determined using an optical interference thickness meter. The surface morphology was examined by field-emission scanning electron microscopy (FE-SEM). The phase purity and twinning were examined using an XRD 2θ–ω scan and ϕ scan of the $10\bar{1}2$ diffraction, respectively. The structural quality was estimated from X-ray rocking curve (XRC) measurements. The impurity concentrations were evaluated using secondary ion mass spectrometry (SIMS).

We also investigated the effect of the gas flow conditions on the shape of the α-Ga_2O_3 islands, which were formed by selective area growth using a SiO_2 mask on *c*-plane sapphire. The mask pattern is shown in Fig. 2. The growth was also conducted in two steps, and the nominal thickness of the second layer (i.e., the thickness of a flat film grown under the same growth conditions) was fixed to be approximately 4 μm. The island shape was observed by FE-SEM.

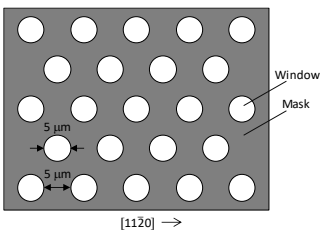

Figure 2. Mask pattern for α-Ga_2O_3 island growth.

3. Results and discussion

3.1 Growth rate vs. F_0(GaCl), F_0(HCl), F_0(O_2)

Figure 3(a) shows the growth rate as a function of F_0(HCl). When F_0(HCl) = 0, the growth rate only gradually increased with increasing F_0(GaCl). During the growth run at F_0(GaCl) = 80 sccm without the additional HCl supply, the inner wall of the rector tube and the substrate holder were covered with white powder, which was formed by the parasitic gas-phase reaction. However, the gas-phase reaction was markedly suppressed by increasing F_0(HCl), and the growth rate increased dramatically. The growth rate began to decrease upon further increase of F_0(HCl).

Figure 3(b) shows the growth rate as a function of F_0(GaCl) under the presence of additional HCl. The growth rate increased monotonically with increasing F_0(GaCl), reaching 101 μm/h. The surface remained specular even at the highest growth rate (Fig. 4).

Figure 3(c) shows the growth rate as a function of F_0(O_2) in the presence of additional HCl. The growth rate first increased with increasing F_0(O_2) and then decreased. At F_0(O_2) = 300 sccm, the flow rate at which the growth rate began to decrease, the formation of white powder was observed.

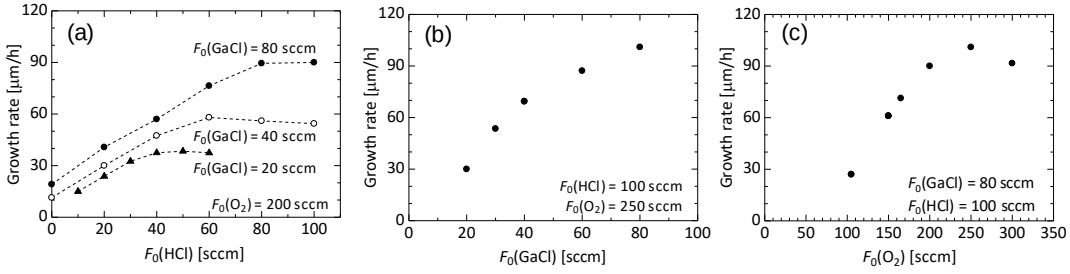

Figure 3. Growth rate of α-Ga_2O_3 as a function of (a) F_0(HCl), (b) F_0(GaCl), and (c) F_0(O_2).

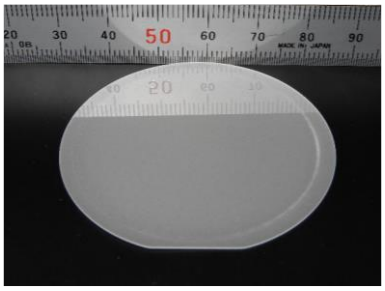

Figure 4. A 2-inch α-Ga_2O_3 epi-wafer grown at ~100 μm/h (F_0(Ga-HCl) = 80 sccm, F_0(HCl) = 100 sccm, $F_0(O_2)$ = 250 sccm).

3.2 Thermodynamic analysis and comparison with experimental results

As described above, the addition of HCl is effective in suppressing the gas-phase reaction, and it is possible to increase the growth rate to a level that cannot be reached only by the optimization of GaCl and O_2 supply. To clarify the mechanism, thermodynamic analysis was utilized to estimate the equilibrium vapor pressures of the gas species in the Group III nozzle of the HVPE reactor (Fig. 1). The calculation procedure is described in Appendix. GaCl, H_2, HCl, and N_2 are supplied in the nozzle. Note that H_2 is the by-product of GaCl, and the feed rate should be 1/2 of F_0(GaCl). Then, equilibrium chemical reaction (1) can occur:

$$GaCl + 2HCl = GaCl_3 + H_2. \quad (1)$$

Figure 5 shows the calculated equilibrium partial pressures as a function of temperature (F_0(GaCl) = 40 sccm, F_0(HCl) = 100 sccm). P_0(X) and P(X) denote the supply partial pressure and equilibrium partial pressure of gas species X, respectively. When the temperature is high enough, almost no $GaCl_3$ is produced, and P(GaCl) remains virtually equal to P_0(GaCl). The equilibrium of (1) moves to the

right-hand side at low temperatures to increase $P(GaCl_3)$ and $P(H_2)$. At 520°C, the growth zone temperature of the present work, 97% of GaCl should be converted into $GaCl_3$. Because H_2 is supplied as a by-product of GaCl and $GaCl_3$ into the growth atmosphere, H_2O should be produced and contribute to the growth as an oxygen source. Therefore, Ga_2O_3 can be produced through the following chemical reactions:

$$2GaCl + 3/2O_2 = Ga_2O_3 + Cl_2 \quad (2)$$

$$2GaCl + 3H_2O = Ga_2O_3 + 2HCl + 2H_2 \quad (3)$$

$$2GaCl_3 + 3/2O_2 = Ga_2O_3 + 3Cl_2 \quad (4)$$

$$2GaCl_3 + 3H_2O = Ga_2O_3 + 6HCl. \quad (5)$$

Note that the contribution fraction of (2)–(5) to the epitaxial growth should be dependent on the ratios of $P_0(GaCl)/P(GaCl_3)$ and VI/III.

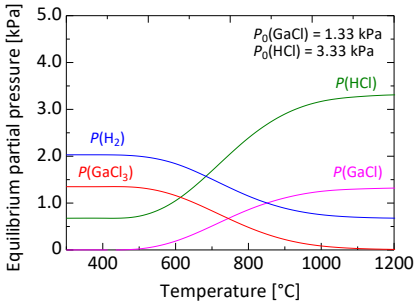

Figure 5. Calculated equilibrium partial pressures of GaCl, H_2, $GaCl_3$, and HCl as a function of temperature.

Figure 6 plots $K_2(T)$–$K_5(T)$, the equilibrium constants of the chemical reactions (2)–(5), as a function of temperature [15]. The fitting parameters when the equilibrium constants are approximated by

$K(T) = a + b/T + c\,log\,T$ are summarized in Table I. $K_4(T)$ and $K_5(T)$ are much smaller than $K_2(T)$ and $K_3(T)$ at approximately 520°C. This finding suggests that the probability of homogeneous nucleation by the gas-phase reaction would be much smaller when $GaCl_3$ is used. Therefore, the conversion of GaCl to $GaCl_3$ with the addition of HCl should be effective to suppress the parasitic reaction, and the experimental results can be explained well with this mechanism. Suppression of the parasitic reaction using $GaCl_3$ was also reported for HVPE of ε-Ga_2O_3, where $GaCl_3$ was produced by the reaction of GaCl and Cl_2 [16, 17].

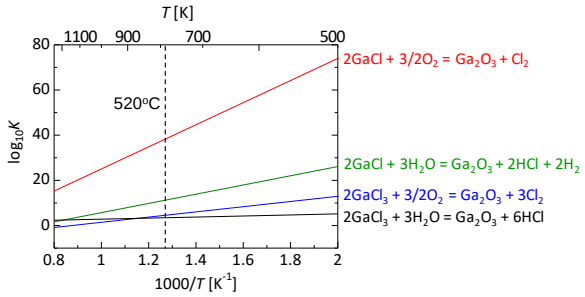

Figure 6. Equilibrium constants of chemical reactions to produce Ga_2O_3 as a function of temperature.

Table I. Fitting parameters for $K_2(T)$–$K_5(T)$

	a	*b*	*c*
$K_2(T)$	3.66×10^1	5.01×10^4	3.84
$K_3(T)$	-3.44×10^1	2.21×10^4	5.89
$K_4(T)$	-3.26	2.28×10^4	-1.20×10^{-1}
$K_5(T)$	-9.45	3.28×10^3	3.00

Figures 7(a)–(c) show the calculated equilibrium partial pressures as a function of P_0(HCl). In any case, conversion of GaCl to $GaCl_3$ proceeds with increasing P_0(HCl). $P(GaCl_3)$ is saturated when P_0(HCl) exceeds $2P_0$(GaCl), and most of the further increase of P_0(HCl) remains unreacted. The

unreacted HCl works as an etching gas to decrease the growth rate. The experimental growth rate data in Fig. 3(a) is replotted in Figs. 7(a)–(c) as a function of P_0(HCl). When P_0(GaCl) = 0.67 kPa (F_0(GaCl) = 20 sccm), the growth rate peak position agrees well with the position at which P($GaCl_3$) levels off and P(HCl) starts rapidly increasing (Fig. 7(a)). However, for higher P_0(GaCl), the growth rate reached a maximum at lower P_0(HCl) than expected (Figs. 7(b), (c)). This result most likely occurs because the actual P($GaCl_3$) saturates at lower P_0(HCl) than expected because of the insufficient gas mixing.

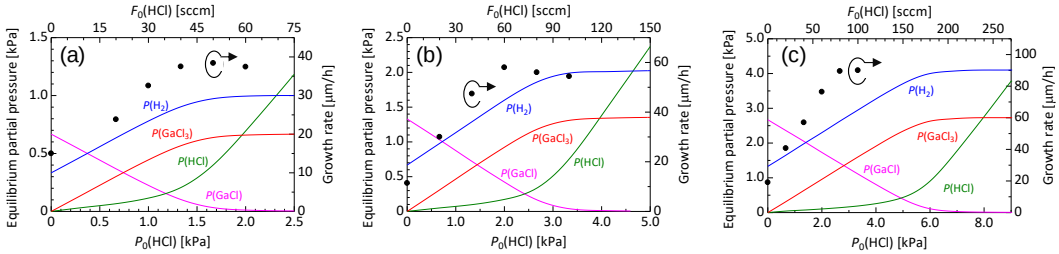

Figure 7. Calculated equilibrium partial pressures of GaCl, H_2, $GaCl_3$, and HCl as a function of P_0(HCl) under fixed P_0(GaCl). (a) P_0(GaCl) = 0.67 kPa (20 sccm), (b) P_0(GaCl) = 1.33 kPa (40 sccm), (c) P_0(GaCl) = 2.67 kPa (80 sccm). The experimental growth rates are also shown. O_2 supply for all the growth was $F_0(O_2)$ = 250 sccm.

Figure 8 shows the calculated equilibrium partial pressures as a function of P_0(GaCl) under the presence of additional HCl. P($GaCl_3$) increases with increasing P_0(GaCl) and levels off because of the shortage of P_0(HCl). Most of the further increase of P_0(GaCl) remains unreacted and directly contributes to the epitaxial growth. The experimental growth rate data in Fig. 3(b) is replotted Fig. 8. The growth rate increased with increasing P_0(GaCl), and the slope decreased when P_0(GaCl) exceeded the point at which P($GaCl_3$) saturated and P(GaCl) started increasing rapidly. This result most likely

occurred because of the decrease in the growth efficiency resulting from the parasitic reaction along with the epitaxial growth through chemical reaction (2) and/or (3).

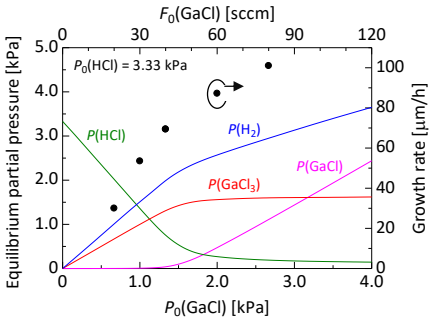

Figure 8. Calculated equilibrium partial pressures of GaCl, H_2, $GaCl_3$, and HCl as a function of P_0(GaCl) under fixed P_0(HCl) = 3.33 kPa (100 sccm). The experimental growth rates are also shown. O_2 supply for all the growth was $F_0(O_2)$ = 250 sccm.

3.3 Surface morphology of flat epilayers

Figures 9(a)–(d) present SEM images of the α-Ga_2O_3 epilayers grown at various F_0(HCl). At F_0(HCl) = 0 sccm (Fig. 9(a)), a large part of the precursors was consumed by the parasitic reaction, and the resulting particles were observed on the surface together with a high density of dimples, which were likely to be formed by the influence of the parasitic reaction. At F_0(HCl) = 60 sccm (Fig. 9(b)), the particles were not observed, but the dimples still existed. At F_0(HCl) = 80 sccm, (Fig. 9 (c)), the surface was smooth. Note that we controlled the gas supply so that the precursors run out a bit earlier than the additional HCl at the end of the growth to suppress the parasitic reaction throughout. The surface roughness increases at the highest HCl supply of F_0(HCl) = 100 sccm (Fig. 9 (d)) was probably because the surface was slightly etched after the growth by residual HCl in the HVPE reactor.

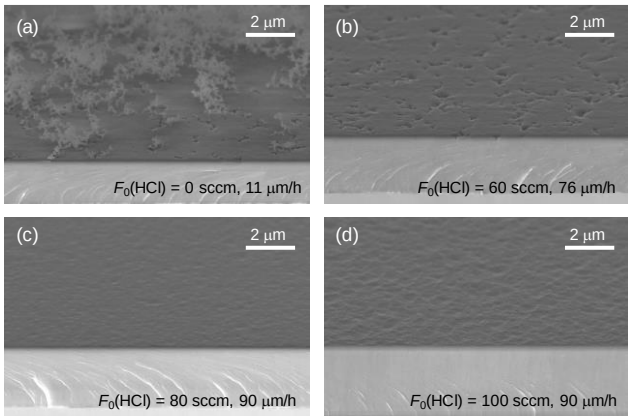

Figure 9. Bird's-eye-view SEM images of α-Ga_2O_3 epilayers grown at (a) F_0(HCl) = 0 sccm, (b) F_0(HCl) = 60 sccm, (c) F_0(HCl) = 80 sccm, and (d) F_0(HCl) = 100 sccm. F_0(GaCl) and F_0(O_2) were fixed at 80 and 200 sccm, respectively.

Figures 10(a)–(c) present SEM images of the α-Ga_2O_3 epilayers grown at various F_0(GaCl). The surface hillocks tended to be larger with increasing F_0(GaCl), although all the sample surfaces were specular to the human eye.

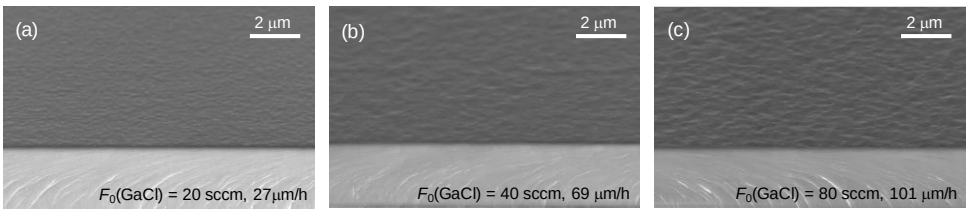

Figure 10. Bird's-eye-view SEM images of α-Ga_2O_3 epilayers grown at (a) F_0(GaCl) = 20 sccm, (b) F_0(GaCl) = 40 sccm, (c) F_0(GaCl) = 80 sccm. F_0(HCl) and F_0(O_2) were fixed at 100 and 250 sccm, respectively.

Figures 11(a)–(d) present SEM images of the α-Ga_2O_3 epilayers grown at various F_0(O_2). The surface hillocks tended to be larger when F_0(O_2) was increased. For F_0(O_2) = 300 sccm, the flow rate at which

growth rate tended to decrease, particles were observed on the surface (Fig. 11(d)) because the HCl supply was not enough to suppress the parasitic reaction. The increase of surface roughness observed in Figs. 10(a)-(c) and Figs. 11 (a)-(c) can be attributed to the nucleation on a terrace, which should be enhanced by the increase of the growth driving force, in addition to the incorporation along a step edge on the epilayer surface.

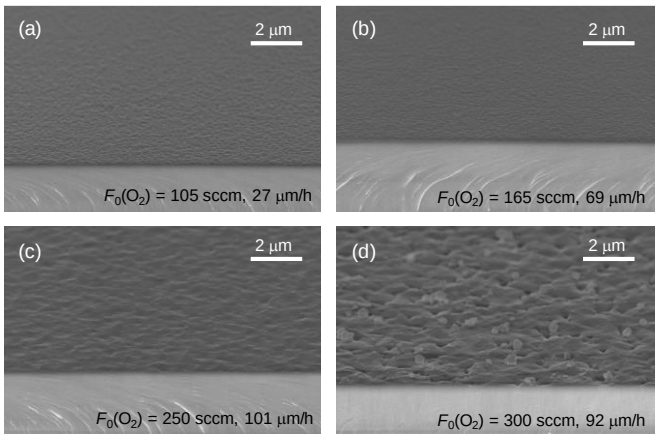

Figure 11. Bird's-eye-view SEM images of α-Ga_2O_3 epilayers grown at (a) $F_0(O_2)$ = 105 sccm, (b) $F_0(O_2)$ = 165 sccm, (c) $F_0(O_2)$ = 250 sccm, (d) $F_0(O_2)$ = 300 sccm. F_0(GaCl) and F_0(HCl) were fixed at 80 and 100 sccm, respectively.

3.4 XRD results

Only diffraction peaks from (0001) plane of α-Ga_2O_3, except those from the substrate, were observed in the XRD 2θ–ω scan profiles (not shown) of all the samples. ϕ-scan profiles of the $10\bar{1}2$ diffraction (not shown) of all the samples exhibited a three-fold symmetric pattern; hence, no twinning was

detected.

Figure 12(a) shows the XRC-FWHMs of the *0006* and $10\bar{1}2$ diffractions, measured in symmetric and skew-symmetric geometries, respectively, as a function of F_0(HCl). The FWHM of the $10\bar{1}2$ diffraction (twist angle) had a minimum near F_0(HCl) = 60 sccm, whereas the FWHM of the *0006* diffraction (tilt angle) behaved in the opposite way. Note that the twist and tilt angles reflect the density of dislocations having screw and edge component, respectively [18, 19].

Figure 12(b) shows the tilt and twist angles as a function of F_0(GaCl). The twist angle decreased with increasing F_0(GaCl), whereas the tilt angle did not show any systematic tendency. The slope of the twist angle decreased above F_0(GaCl) = 40 sccm, the flow rate at which P_0(GaCl) started increasing rapidly in Fig. 8. This tendency implies that the use of $GaCl_3$ would be better than the use of GaCl from the viewpoint of structural quality.

Figure 12(c) shows the tilt and twist angles as a function of $F_0(O_2)$. The twist angle decreased with increasing $F_0(O_2)$, whereas the tilt angle did not show any systematic tendency. However, improvement of the twist angle leveled off at $F_0(O_2)$ = 300 sccm, a flow rate at which the parasitic reaction was obvious.

The twist angles in Figs. 12(a)–(c) are replotted in Fig. 12(d) as a function of growth rate. The twist angle decreased with increasing growth rate when the growth rate was controlled using F_0(GaCl) or $F_0(O_2)$ as the parameters. At the same growth rate, the structural quality was better when the VI/III

ratio was higher. In general, crystal quality tends to be worse in most cases when the growth rate is too high. However, the opposite tendency was observed in the present work. This tendency could be attributed to the increase of surface roughness at high growth rates. In general, dislocation lines tend to be perpendicular to the crystal surface to minimize the elastic energy. Accordingly, the dislocation lines bend when they meet inclined surface to annihilate by making dislocation loops. As a result, density of dislocations propagating along the film normal direction can be decreased. This principle has been widely utilized to produce high-quality GaN crystals [20], and also applied to α-Ga_2O_3 [14]. In addition, nucleation on a terrace and coalescence of the nuclei, which are likely to be enhanced under large growth driving force, would cause tensile strain to reduce surface energy [21], and such tensile strain could work to reduce the crystal volume through the elimination of extra half plains, leading to the reduction of edge dislocation density. To clarify the mechanism of the quality improvement in the present case, we are preparing cross-sectional TEM to observe the behavior of dislocations in the high-speed grown samples. The results would be published elsewhere. When F_0(HCl) was used as the parameter, the twist angle decreased with increasing the growth rate, then reached a minimum at approximately 80 μm/h. In this case, the crystal quality could be in a trade-off relationship between the formation/suppression of unexpected particles formed by the parasitic reaction and the “rough-surface effect” described above.

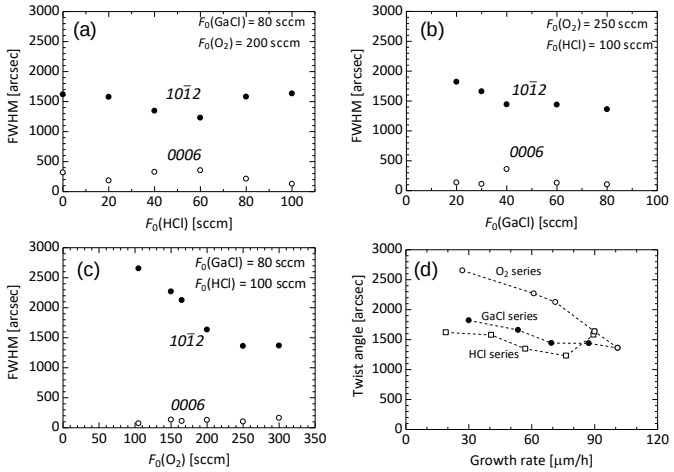

Figure 12. XRC-FWHMs as a function of (a) F_0(HCl), (b) F_0(GaCl), (c) F_0(O$_2$). (d) XRD-FWHM as a function of growth rate.

3.5 Impurity analysis by SIMS

SIMS measurements were performed to clarify the effect of F_0(X) on the impurity concentrations in the unintentionally doped α-Ga_2O_3 epilayers. The measured elements and detection limits are summarized in Table II. Of the measured elements, only H and Cl were detected. Figures 13(a)–(b) show [H] and [Cl] as a function of F_0(GaCl) and F_0(O$_2$), respectively. Both [H] and [Cl] increased with increasing F_0(GaCl) or F_0(O$_2$), and [Cl] increased more rapidly. These results are replotted in Fig. 13(c) as a function of growth rate. Both [H] and [Cl] increased with increasing the growth rate. This tendency can be attributed to the decrease in the desorption probability of the H or Cl species from the surface at high growth rates. We expected that [H] and [Cl] would be higher for lower VI/III ratios, as the partial pressures of the potential Cl source ($GaCl_3$) and H source (H_2) would be higher. In the case of MOVPE of GaN, carbon doping can be controlled using V/III (NH_3/TMGa, for example) ratio as a

parameter. The metalorganic (MO) precursors are thermally unstable at GaN growth temperatures, and therefore they decompose to release the carbon source, i.e., hydrocarbon fragments [22]. As a result, the carbon concentration in GaN increases with decreasing the V/III ratio [23]. However, in the present case, both [H] and [Cl] appeared to be dominated only by the growth rate as they appeared on a single curve regardless of the VI/III ratio. This is probably because the possible sources of H and Cl, i.e., H_2O and $GaCl_x$, respectively, are stable at the growth temperatures, and therefore the species can contribute to the unintentional doping only when they take part in the crystal growth on the surface in contrast to the case of carbon doping in MOVPE-GaN, in which hydrocarbon fragments can be supplied from all the MO molecules present in the growth atmosphere.

Table II. Measured elements and detection limits of SIMS

Element	H	C	N	Si	S	Cl
D. L. [cm^{-3}]	5×10^{16}	5×10^{16}	5×10^{15}	2×10^{15}	5×10^{15}	2×10^{15}

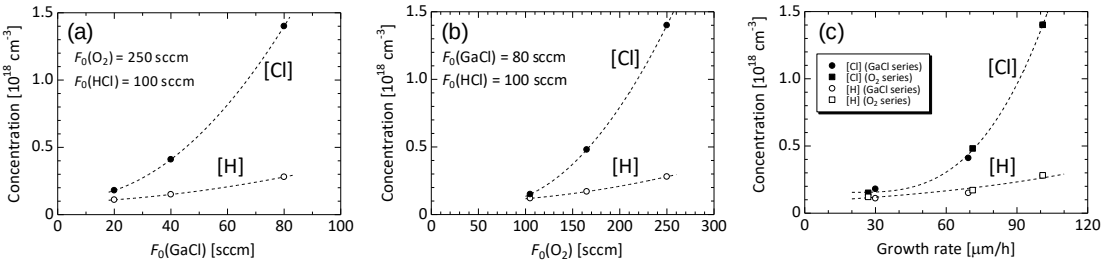

Figure 13. Concentrations of H and Cl impurities as a function of (a) F_0(GaCl), (b) $F_0(O_2)$. (c) Concentrations of H and Cl as a function of growth rate.

3.6 Island morphology

Figures 14(a)–(f) present SEM images of the α-Ga_2O_3 islands grown on a sapphire substrate with a SiO_2 mask on top under various F_0(GaCl). α-Ga_2O_3 islands were successfully grown even at the highest growth rate of 101 μm/h. Under smaller F_0(GaCl) condition, the lateral/vertical growth rate ratio tended to be smaller, and the vertical $(11\bar{2}0)$ facet area increased. Nucleation of polycrystal grains was observed on the mask when $F_0(\mathrm{GaCl}) \geq 40$ sccm. Although the nucleation was also observed on the island facets when F_0(GaCl) = 80 sccm, it was limited to the bottom part of the islands, and therefore, such grains should be buried soon.

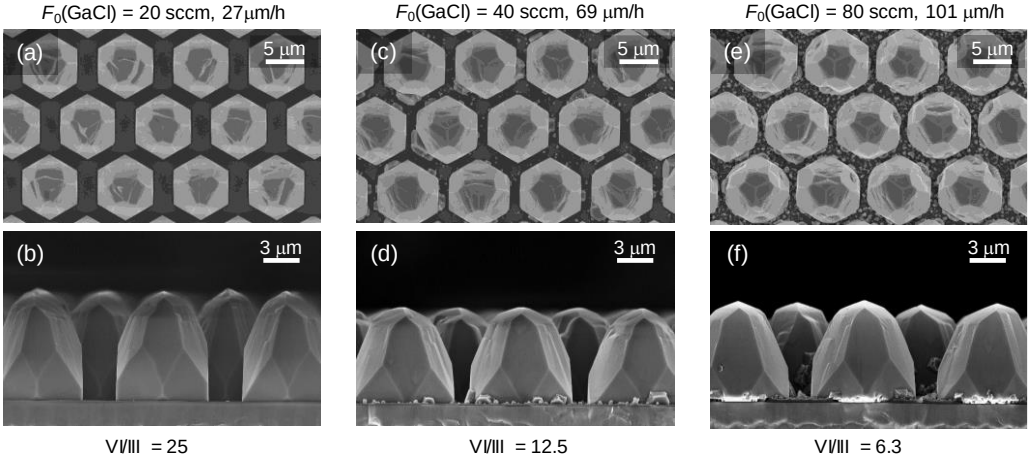

Figure 14. SEM images of α-Ga_2O_3 islands grown at (a), (b) F_0(GaCl) = 20 sccm, (c), (d) F_0(GaCl) = 40 sccm, (e), (f) F_0(GaCl) = 80 sccm. F_0(HCl) and $F_0(O_2)$ were fixed at 100 and 250 sccm, respectively. Note that VI/III = $2F_0(O_2)/F_0$(GaCl).

Figures 15(a)–(f) present SEM images of the α-Ga_2O_3 islands grown on a sapphire substrate with a SiO_2 mask on top under various $F_0(O_2)$ conditions. For smaller $F_0(O_2)$, the lateral/vertical growth rate ratio tended to be smaller. Comparing Figs. 15(a)–(b) and Figs. 14(a)–(b) (both grown at 27 μm/h)

and Figs. 15(c)–(d) and Figs. 14(c)–(d) (both grown at 69 μm/h), it was observed that the $(10\bar{1}4)$ facet area on the island top was smaller under lower VI/III conditions and the nucleation density on the mask was smaller.

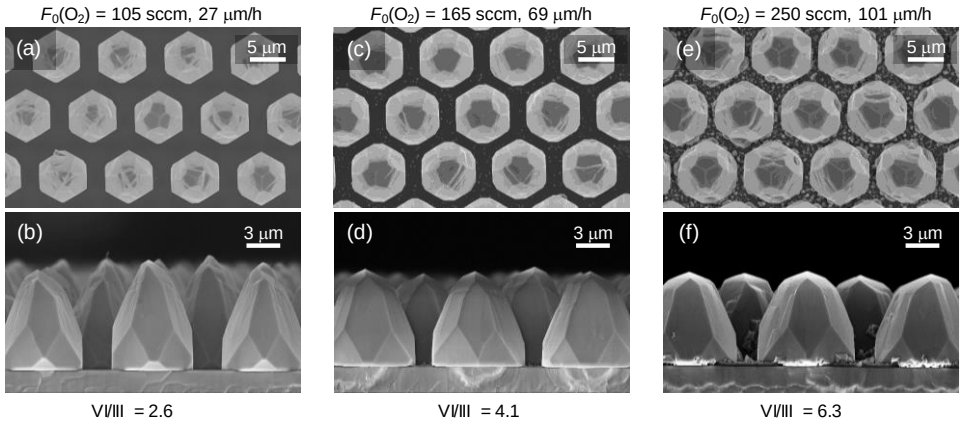

Figure 15. SEM images of α-Ga_2O_3 islands grown at (a), (b) $F_0(O_2)$ = 105 sccm, (c), (d) $F_0(O_2)$ = 165 sccm, and (e), (f) $F_0(O_2)$ = 250 sccm. F_0(GaCl) and F_0(HCl) were fixed at 80 and 100 sccm, respectively. Note

In general, growth morphology of a crystal is determined by the growth rate ratio between the crystal planes, and a crystal plane with slower growth rate should have larger area [24]. The growth rate ratio can be discussed in terms of incorporation efficiency of constituent atoms, which should be sensitively affected by the microscopic surface structure and the growth conditions such as temperature and degree of super saturation, etc. [24, 25]. However, the island morphology observed here may not be intrinsic because they were closely adjacent with each other. For example, the reduction in the lateral/vertical growth rate ratio at lower precursor supply is likely because a large part of precursors was consumed at the upper facets and only a limited amount was supplied to the bottom parts,

evidenced by the decrease of nucleation on the mask with decreasing the precursor supply observed in Figs. 14 and 15. The intrinsic morphology needs to be investigated in a future work. For this purpose, the distance between islands need to be large enough so that precursors are supplied uniformly.

4. Summary

We investigated the effect of the precursor supply and additional HCl on the HVPE growth rate and crystal properties of α-Ga_2O_3. The parasitic gas-phase reaction was suppressed by supplying HCl in addition to the precursors, and a very high growth rate as high as 101 μm/h was achieved. Thermodynamic analysis revealed that the addition of HCl works to convert GaCl into $GaCl_3$, and the parasitic reaction was suppressed because α-Ga_2O_3 was grown via the chemical reaction of $GaCl_3$ and the oxygen sources, the equilibrium constant of which is much smaller than that when GaCl is used. All the α-Ga_2O_3 epilayers grown in the present work were confirmed to be phase-pure and twin-free by XRD regardless of the VI/III ratio or growth rate. The twist angle decreased with increasing growth rate by controlling F_0(GaCl) or F_0(O_2), whereas the tilt angle did not show any systematic tendency. H and Cl impurities were detected by SIMS in all the samples investigated in the present work. [C], [N], [Si], and [S] were below the detection limits. [H] and [Cl] increased with increasing growth rate, reaching 3 x 10^{17} cm^{-3} and 1.4 x 10^{18} cm^{-3}, respectively, at 101 μm/h. At the same growth rate, changing the VI/III ratio did not affect [H] or [Cl]. α-Ga_2O_3 islands were successfully formed by selective area growth using a SiO_2 mask even at 101 μm/h. The lateral/vertical growth rate ratio of the

islands increased with increasing F_0(GaCl) or F_0(O_2). The $(10\bar{1}4)$ facet area become smaller and parasitic nucleation on the mask decreased at lower VI/III ratios at the same growth rate.

5. Appendix: Thermodynamic analysis

GaCl, H_2, HCl, and N_2 were supplied in the group III nozzle of the HVPE reactor, and chemical reaction (1) occurred:

$GaCl + 2HCl = GaCl_3 + H_2$. (1)

The equilibrium constant $K_1(T)$ of this reaction is approximated as follows [26]:

$$\log K_1(T) = -5.54 + \frac{8.93 \times 10^3}{T} - 5.70 \times 10^{-1} \log T \quad \text{(i)}$$

The law of mass action is expressed as follows:

$$\frac{P(GaCl_3)P(H_2)}{P(GaCl)P(HCl)^2} = K(T) \quad \text{(ii)}$$

Because the growth occurs under atmospheric pressure,

$$P(GaCl) + P(HCl) + P(GaCl_3) + P(H_2) + P(N_2) = 100 \text{ kPa} \quad \text{(iii)}$$

The molar decrease of GaCl and molar increase of $GaCl_3$ should be the same:

$$P_0(GaCl) - P(GaCl) = P(GaCl_3) - P_0(GaCl_3) \quad \text{(iv)}$$

The molar increases of $GaCl_3$ and H_2 should be equal:

$$P(GaCl_3) - P_0(GaCl_3) = P(H_2) - P_0(H_2) \quad \text{(v)}$$

The molar decrease of HCl should be twice the molar decrease of GaCl:

$$P_0(HCl) - P(HCl) = 2\{P_0(GaCl) - P(GaCl)\} \qquad \text{(vi)}$$

The equilibrium partial pressures of P(GaCl), P(HCl), $P(GaCl_3)$, $P(O_2)$ can be determined by solving the simultaneous equations (ii)–(vi).

Acknowledgements

Part of this work was supported by Innovative Science and Technology Initiative for Security, ATLA, Japan.

References

[1] D. Shinohara and S. Fujita, Jpn. J. Appl. Phys. **47**, 7311 (2008).

[2] M. Oda, R. Tokuda, H. Kambara, T. Tanikawa, T. Sasaki, and T. Hitora: Appl. Phys. Express **9**, 021101 (2016).

[3] S. Fujita and K. Kaneko, J. Cryst. Growth **401**, 588 (2014).

[4] R. Miller, F. Alema, and A. Osinsky, IEEE Trans. Semicond. Manufacturing, **31**, 467 (2018).

[5] K. Kaneko, S. Fujita, and T. Hitora, Jpn. J. Appl. Phys. **57**, 02CB18 (2018).

[6] FLOSFIA and Kyoto univ: News release, July 13 (2008). http://flosfia.com/20180713/

[7] Y. Oshima, E. G. Villora, and K. Shimamura, Appl. Phys. Express **8**, 055501 (2015).

[8] A. I. Pechnikov, S. I. Stepanov, A. V. Chikiryaka, M. P. Scheglov, M. A. Odnobludov, and V. I. Nikolaev, Semiconductors **53**, 780 (2019).

[9] H. Son and D. W. Jeon, J. Alloys Compd. **773**, 631 (2019)

[10] Z. Cheng, M. Hanke, P. Vogt, O. Bierwagen, and A. Trampert, Appl. Phys. Lett. 111, 162104 (2017).

[11] R. Jinno, Y. Cho, K. Lee, V. Protasenko, H. G. Xing, and D. Jena, "Stabilization of α-Ga_2O_3 on m-plane α-Al_2O_3 by Plasma-Assisted MBE" Paper presented at 66th JSAP spring meeting, Tokyo, Japan, 9-12 March (2019).

[12] H. Sun, K-H. Li, C. G. Torres Castanedo, S. Okur, G. S. Tompa, T. Salagaj, S. Lopatin, A. Genovese, and X. Li, Cryst. Growth Des. **18**, 2370 (2018).

[13] D. Machon, P. F. McMillan, B. Xu, and J. Dong, Phys. Rev. B **73**, 094125, (2006).

[14] Y. Oshima, K. Kawara, T. Shinohe, T. Hitora, M. Kasu, S. Fujita, APL mater. **7**, 022503 (2019).

[15] K. Nomura, K. Goto, R. Togashi, H. Murakami, Y. Kumagai, A. Kuramata, S. Yamakoshi, and A. Koukitu, J. Cryst. Growth **405**, 19 (2014).

[16] M. Sato, N. Takekawa, H. Murakami, Y. Kumagai, "Comparison between GaCl-O_2-N_2 and $GaCl_3$-O_2-N_2 systems in ε-Ga_2O_3 Vapor Phase Epitaxy", Ext. Abstr. (66th Spring Meet., 2019); Japan Society of Applied Physics, 11p-S011-1 [in Japanese].

[17] K. Ema, N. Takekawa, K. Goto, H. Murakami, and Y. Kumagai, "Growth of *ε*-Ga_2O_3 on *a*-plane Sapphire Substrate by Tri-Halide Vapor Phase Epitaxy", Ext. Abstr. (80th Fall Meet., 2019); Japan Society of Applied Physics, 21p-B31-7 [in Japanese].

[18] P. Gay, P. B. Hirsch and A. Kelly, Acta metall. 1, 315 (1953).

[19] T. C. Ma, X. H. Chen , Y. Kuang, L. Li, J. Li, F. Kremer , F.-F. Ren, S. L. Gu, R. Zhang, Y. D. Zheng, H. H. Tan , C. Jagadish, and J. D. Ye, Appl. Phys. Lett. **115**, 182101 (2019).

[20] A. Usui, H. Sunakawa, A. Sakai, and A. A. Yamaguchi, Jpn. J. Appl. Phys. **36**, L899 (1997).

[21] T. Böttcher, S. Einfeldt, S. Figge, R. Chierchia, H. Heinke and D. Hommel, Appl. Phys. Lett. **78**, 1976 (2001).

[22] H.-T. Lam, J.M. Vohs, Surf. Sci. 426, **199** (1999).

[23] D. D. Koleske, A. E. Wickenden, R. L. Henry, M. E. Twigg, J. Cryst. Growth **242**, 55 (2002).

[24] I. Sunagawa, *Crystals: Growth, Morphology, & Perfection* (Cambridge University Press, Cambridge, 2007, ISBN: 9780521714792), Chapter 2 and 3.

[25] K. Hiramatsu, K. Nishiyama, M. Onishi, H. Mizutani, M. Narukawa, A. Motogaito, H Miyake, Y. Iyechika, T. Maeda, J. Cryst. Growth **221**, 316 (2000).

[26] A. Koukitu, S. Hama, T. Taki, and H. Seki, Jpn. J. Appl. Phys. **37**, 762 (1998).

Figure captions

Fig. 1. Schematic illustration of HVPE reactor and temperature profile.

Fig. 2. Mask pattern for α-Ga_2O_3 island growth.

Fig. 3. Growth rate of α-Ga_2O_3 as a function of (a) F_0(HCl), (b) F_0(GaCl), and (c) $F_0(O_2)$.

Fig. 4. A 2-inch α-Ga_2O_3 epi-wafer grown at ~100 μm/h (F_0(Ga-HCl) = 80 sccm, F_0(HCl) = 100 sccm,

$F_0(O_2)$ = 250 sccm).

Fig. 5. Calculated equilibrium partial pressures of GaCl, H_2, $GaCl_3$, and HCl as a function of temperature.

Fig. 6. Equilibrium constants of chemical reactions to produce Ga_2O_3 as a function of temperature.

Fig. 7. Calculated equilibrium partial pressures of GaCl, H_2, $GaCl_3$, and HCl as a function of P_0(HCl) under fixed P_0(GaCl). (a) P_0(GaCl) = 0.67 kPa (20 sccm), (b) P_0(GaCl) = 1.33 kPa (40 sccm), (c) P_0(GaCl) = 2.67 kPa (80 sccm). The experimental growth rates are also shown. O_2 supply for all the growth was $F_0(O_2)$ = 250 sccm.

Fig. 8. Calculated equilibrium partial pressures of GaCl, H_2, $GaCl_3$, and HCl as a function of P_0(GaCl) under fixed P_0(HCl) = 3.33 kPa (100 sccm). The experimental growth rates are also shown. O_2 supply for all the growth was $F_0(O_2)$ = 250 sccm.

Fig. 9. Bird's-eye-view SEM images of α-Ga_2O_3 epilayers grown at (a) F_0(HCl) = 0 sccm, (b) F_0(HCl) = 60 sccm, (c) F_0(HCl) = 80 sccm, and (d) F_0(HCl) = 100 sccm. F_0(GaCl) and $F_0(O_2)$ were fixed at 80 and 200 sccm, respectively.

Fig. 10. Bird's-eye-view SEM images of α-Ga_2O_3 epilayers grown at (a) F_0(GaCl) = 20 sccm, (b) F_0(GaCl) = 40 sccm, (c) F_0(GaCl) = 80 sccm. F_0(HCl) and $F_0(O_2)$ were fixed at 100 and 250 sccm, respectively.

Fig. 11. Bird's-eye-view SEM images of α-Ga_2O_3 epilayers grown at (a) $F_0(O_2)$ = 105 sccm, (b) $F_0(O_2)$

= 165 sccm, (c) $F_0(O_2)$ = 250 sccm, (d) $F_0(O_2)$ = 300 sccm. F_0(GaCl) and F_0(HCl) were fixed at 80 and 100 sccm, respectively.

Fig. 12. XRC-FWHMs as a function of (a) F_0(HCl), (b) F_0(GaCl), (c) $F_0(O_2)$. (d) XRD-FWHM as a function of growth rate.

Fig. 13. Concentrations of H and Cl impurities as a function of (a) F_0(GaCl), (b) $F_0(O_2)$. (c) Concentrations of H and Cl as a function of growth rate.

Fig. 14. SEM images of α-Ga_2O_3 islands grown at (a), (b) F_0(GaCl) = 20 sccm, (c), (d) F_0(GaCl) = 40 sccm, (e), (f) F_0(GaCl) = 80 sccm. F_0(HCl) and $F_0(O_2)$ were fixed at 100 and 250 sccm, respectively. Note that VI/III = $2F_0(O_2)/F_0$(GaCl).

Fig. 15. SEM images of α-Ga_2O_3 islands grown at (a), (b) $F_0(O_2)$ = 105 sccm, (c), (d) $F_0(O_2)$ = 165 sccm, and (e), (f) $F_0(O_2)$ = 250 sccm. F_0(GaCl) and F_0(HCl) were fixed at 80 and 100 sccm, respectively. Note that (e) and (f) are the same images as Figs. 14(e) and (f), respectively.